

---

This is an electronic reprint of the original article.  
This reprint may differ from the original in pagination and typographic detail.

Xue, Bing; Haneda, Katsuyuki; Icheln, Clemens

## Evaluation of Base Station Antenna Arrays for In-Band Full Duplex Communications

*Published in:*  
EuCAP 2025 - 19th European Conference on Antennas and Propagation

*DOI:*  
[10.23919/EuCAP63536.2025.10999867](https://doi.org/10.23919/EuCAP63536.2025.10999867)

Published: 01/01/2025

*Document Version*  
Peer-reviewed accepted author manuscript, also known as Final accepted manuscript or Post-print

*Please cite the original version:*  
Xue, B., Haneda, K., & Icheln, C. (2025). Evaluation of Base Station Antenna Arrays for In-Band Full Duplex Communications. In *EuCAP 2025 - 19th European Conference on Antennas and Propagation* IEEE.  
<https://doi.org/10.23919/EuCAP63536.2025.10999867>

---

This material is protected by copyright and other intellectual property rights, and duplication or sale of all or part of any of the repository collections is not permitted, except that material may be duplicated by you for your research use or educational purposes in electronic or print form. You must obtain permission for any other use. Electronic or print copies may not be offered, whether for sale or otherwise to anyone who is not an authorised user.

# Evaluation of Base Station Antenna Arrays for In-Band Full Duplex Communications

Bing Xue\*, Katsuyuki Haneda\*, Clemens Icheln\*

\*Department of Electronics and Nanoengineering, Aalto University-School of Electrical Engineering, Espoo, Finland, E-mail: bing.xue@aalto.fi

**Abstract**—This paper investigates the achievable rates of in-band full-duplex antenna arrays within a limited area by varying numbers of antenna elements. Patch and dipole antenna arrays with  $\pm 45^\circ$  and  $0^\circ - 90^\circ$  element configurations are compared based on their mutual coupling levels. Among them, the dipole antenna array with a  $\pm 45^\circ$  element distribution is selected for calculating the channel capacities of in-band full-duplex systems with varying numbers of antenna elements, all within a limited area. The optimal element spacing is determined to be 0.5 wavelength at both 2.6 GHz and 7.5 GHz. Radiation patterns and S-parameters of the fabricated antenna array are measured at 3.6 GHz. These measured radiation patterns are then used to compute the achievable Rates for in-band full-duplex operation, further supporting the study's conclusions.

**Index Terms**—Antenna array, In-band Full duplex, Base station antenna, achievable Rates.

## I. INTRODUCTION

Wireless communication is important in everyone's daily life. In order to pursue high-rate communications, researchers have proposed different duplex-mode realizations [1]. Among them, in-band full-duplex, in which transmission and reception occur at the same time and in the same frequency band, has the potential to as much as double the spectral efficiency of traditional half-duplex systems [2], as shown in Fig. 1. Researchers have used digital beamforming in addition to analog beamforming to reduce self-interference, which is the main challenge limiting the application of in-band full-duplex between the transmitters and receivers in the base station [2]–[6]. Base stations have limited physical space for placing antennas, which restricts the number of antennas and their spacing. When only a few antennas are placed within a limited area, mutual coupling between antennas is reduced, which in turn minimizes the need for digital self-interference reduction resources. However, this comes at the cost of reduced achievable rates. On the other hand, increasing the number of antennas can improve achievable rates but requires more resources to mitigate digital self-interference. Consequently, there is insufficient information regarding the optimal number of in-band full-duplex antenna arrays that can be effectively deployed within a limited space.

This paper begins by discussing the selection of antenna types and distribution approaches, followed by the design of antenna elements and arrays at 2.6 GHz within a limited area. Next, the calculation model for in-band full-duplex with digital beamforming is introduced, and the calculations are performed at 2.6 GHz and extended to 7.5 GHz. Finally, the radiation patterns and S-parameters of the fabricated antenna array at

3.6 GHz are measured, and the measured radiation patterns are used to calculate the achievable rates of the in-band full-duplex system, validating the calculations.

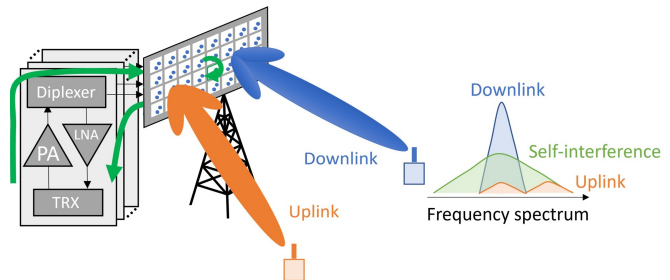


Fig. 1. The self-interference schematic of an in-band full duplex base-station antenna array.

## II. ANTENNA ARRAY DESIGN

In order to reduce the self-interference between the uplink and downlink, the straightforward approach is to lower the mutual coupling levels between antennas. For classical base-station antenna arrays, patch antennas [7], [8] and dipole antennas [9], [10] are two suitable options since they share the aperture for two orthogonal polarizations with high polarization isolation. When creating an array, self-interference also arises from the mutual coupling of different elements. There are two methods to distribute antenna elements, namely,  $\pm 45^\circ$  and  $0^\circ - 90^\circ$  distributions, as shown in Fig. 2. Through full-wave simulations, we can determine which type of antennas and distributions contribute to the lowest mutual coupling levels between antennas. We implemented full-wave simulations at 2.6 GHz for a dipole and patch  $3 \times 3$  antenna array with  $\pm 45^\circ$  and  $0^\circ - 90^\circ$  distributions, respectively. The spacing between antenna elements is  $d_0 = 0.4\lambda_0$ , where  $\lambda_0$  is the free-space wavelength at 2.6 GHz. We can make a comparison

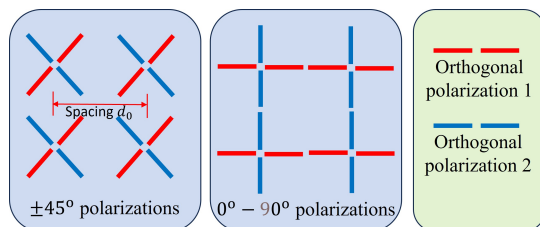


Fig. 2. Schematic of  $2 \times 2$  antenna element distributions in an array.

among these four cases, as shown in Table I. It can be observed that the dipole array with  $\pm 45^\circ$  distribution provides the

highest isolation and the largest bandwidth. Therefore, in the following studies, we use dipoles to design the antenna arrays.

TABLE I  
PERFORMANCE COMPARISONS FOR FOUR CASES AT  $d_0 = 0.4\lambda_0$

	-10 dB bandwidth	Maximum mutual coupling
Patch ( $0^\circ - 90^\circ$ )	> 15%	-6.7 dB
Patch ( $\pm 45^\circ$ )	> 15%	-10.5 dB
Dipole ( $0^\circ - 90^\circ$ )	> 35%	-7.2 dB
Dipole ( $\pm 45^\circ$ )	> 35%	-13.5 dB

### A. Element Design

The substrate is 1 mm thick FR4, with a dielectric constant of 4.3 and a loss tangent of 0.016. The metal layer thickness is 18  $\mu\text{m}$ . The two orthogonal dipoles are fed by two coaxial cables with a 0.15 mm-diameter center pin and a 1.19 mm-diameter outer shield. The center pin is connected to the top metal layer, while the outer shield is connected to the bottom layer, as shown in Fig. 3. The dimensions of the antenna

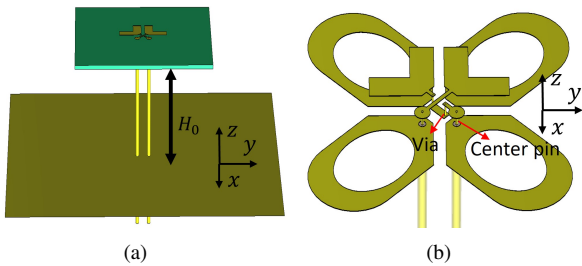


Fig. 3. (a) Side view of dual-polarized dipole antennas with coaxial cable feeds. (b) Side view of the antennas with the hidden substrate.  $H_0 = 28.75$  mm. The radius of the vias is 0.1 mm.

working at 2.6 GHz on the substrate are shown in Fig. 4. The reflection coefficients and mutual coupling levels of the

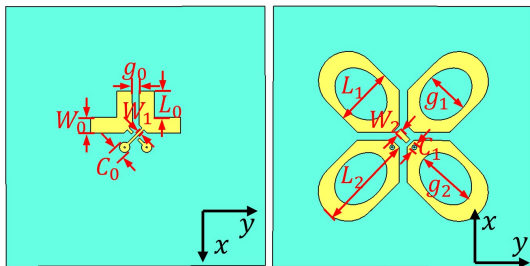


Fig. 4. Top and bottom views of the substrate.  $g_0 = 1$  mm;  $W_0 = 3$  mm;  $L_0 = 5.06$  mm;  $C_0 = 2$  mm;  $W_1 = 0.5$  mm;  $g_1 = 8.4$  mm;  $g_2 = 11.4$  mm;  $L_1 = 11.4$  mm;  $L_2 = 18.7$  mm;  $C_1 = 0.94$  mm;  $W_2 = 0.5$  mm.

dual-polarized antennas are shown in Fig. 5(a), and the 3D radiation pattern of one antenna is shown in Fig. 5(b), as the other antenna has a nearly identical radiation pattern. The -10 dB impedance bandwidth is > 600 MHz, and the mutual coupling level between the two antennas is below -29 dB at 2.6 GHz. The realized gain of the antenna is approximately 8 dBi.

### B. Array Design

By using the antenna element designed in Section II-A, we create an antenna array within a limited area of  $300 \times 600$  mm<sup>2</sup>. The antenna distributions are based on Fig. 2, i.e., a dipole

antenna array with the  $\pm 45^\circ$  distribution. We vary the number of antenna elements from  $1 \times 2$  to  $6 \times 12$  with spacing from  $2.6\lambda_0$  to  $0.43\lambda_0$ , where  $\lambda_0$  is the free-space wavelength at 2.6 GHz. Fig. 6 shows an example of a  $5 \times 10$  antenna array with 100 antenna feeds.

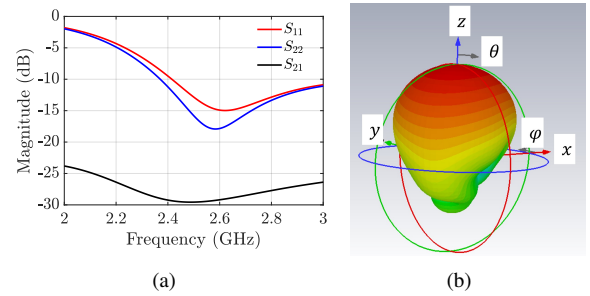


Fig. 5. (a) Simulated S-parameters of the dual-polarized antennas. (b) Radiation pattern of one antenna.

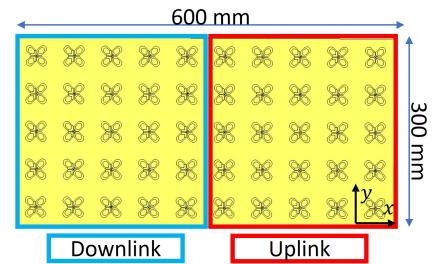


Fig. 6.  $5 \times 10$  antenna array with 100 antenna feeds. The substrate is hidden.

## III. IN-BAND FULL DUPLEX

### A. Calculation Model

There are different allocations for uplink and downlink sub-arrays in an in-band full-duplex antenna array, such as West-East, North-South, Northwest-Southeast, and Interleaved, as shown in [2, Fig.7]. Based on the conclusions in [2], the West-East distribution is the best for the  $300 \times 600$  mm<sup>2</sup> area, as shown in Fig. 6, where the left and right parts belong to downlink and uplink sub-arrays, respectively. In this distribution, the main self-interference results from the antennas in the downlink sub-array near the uplink sub-array.

The signals' strength meets the Rayleigh fading. In other words, these signals  $(p(\theta, \phi) = \frac{1}{\sqrt{2}}(x + jy))$  are independent and identically distributed (i.i.d.) zero-mean complex Gaussian variables with unit variance. Therefore, we have  $h_n$  to describe the channel [11] written as

$$h_n = \frac{\exp(-jk_0 d)}{d} \int \sqrt{G_{0,i}(\theta_0, \phi_0)} p(\theta, \phi) \sin \theta d\theta d\phi, \quad (1)$$

where  $k_0$  is the free space wave number,  $n$  is the  $n$ -th antenna in the array, and  $d$  is the distance between the user and the base-station antenna array.

The goal of the signaling scheme in this paper is to project the strong self-interference onto their noise subspace while using maximum-ratio-combining and precoding for the uplink and downlink channels without considering their alignment with the self-interference. Therefore, the self-interference reduction algorithm in [12] is applied in this paper. It is assumed

that each mobile user has one single antenna. We define the precoders,  $\mathbf{P}_r$  and  $\mathbf{P}_t$  [12]. Then the signal obtained after coding at the base station is

$$\hat{\mathbf{y}}_{\text{up}} = \mathbf{P}_r \mathbf{H}_{\text{up}} \mathbf{x}_{\text{up}} + \mathbf{P}_r \mathbf{H}_{\text{self}} \mathbf{P}_t \mathbf{x}_{\text{down}} + \mathbf{P}_r \mathbf{n}_{\text{up}}, \quad (2)$$

where  $\mathbf{H}_{\text{self}} \in \mathbb{C}^{M_{\text{up}} \times M_{\text{down}}}$ ,  $\mathbf{H}_{\text{up}} \in \mathbb{C}^{M_{\text{up}} \times K_{\text{up}}}$  is the uplink channel matrix,  $\mathbf{x}_{\text{down}}$  and  $\mathbf{x}_{\text{up}}$  are the vector of symbols transmitted by and received by the base station, and  $\mathbf{n}_{\text{up}} \in \mathbb{C}^{M_{\text{up}}}$  is the noise at receiving antennas in base station.  $M_{\text{up}}$  and  $M_{\text{down}}$  are the number of the transmitting and receiving antennas in the base station.  $K_{\text{up}}$  is the number of the uplink users. If we select the eigen-beamforming, by using  $\mathbf{H}_{\text{self}} = \mathbf{U} \mathbf{\Sigma} \mathbf{V}^H$ , we can obtain  $\mathbf{P}_r = \mathbf{S}_r^T \mathbf{U}^H$  and  $\mathbf{P}_t = \mathbf{V} \mathbf{S}_t$ , where  $\mathbf{S}_r^T \in \{0, 1\}^{N_{\text{up}} \times M_{\text{up}}}$  and  $\mathbf{S}_t \in \{0, 1\}^{M_{\text{down}} \times N_{\text{down}}}$ , and  $N_{\text{up}}$  and  $N_{\text{down}}$  are the number of effective antennas for uplink and downlink, respectively [2]. By minimizing the self-interference term, one strategy is to choose [12]:

$$\mathbf{S}_r^T = \begin{bmatrix} \mathbf{0} & \mathbf{I}_{N_{\text{up}}} \end{bmatrix} \text{ and } \mathbf{S}_t = \begin{bmatrix} \mathbf{0} \\ \mathbf{I}_{N_{\text{down}}} \end{bmatrix}. \quad (3)$$

Similarly, when the interference caused by uplink users on downlink reception is minimized, we assume no interference between users [2]. In this way, we can focus only on the self-interference at the base station. The precoded signal received by users is

$$\hat{\mathbf{y}}_{\text{down}} = \mathbf{H}_{\text{down}} \mathbf{P}_{\text{ZF}} \mathbf{P}_t \mathbf{x}_{\text{down}} + \mathbf{n}_{\text{down}}, \quad (4)$$

where  $\mathbf{H}_{\text{down}} \in \mathbb{C}^{K_{\text{down}} \times M_{\text{down}}}$ ;  $\mathbf{n}_{\text{down}} \in \mathbb{C}^{K_{\text{down}}}$  is the noise at  $K_{\text{down}}$  downlink users;  $\mathbf{P}_{\text{ZF}}$  is the precoder for zero-forcing beamforming [2].

Formulas (14) and (15) in [2] can be used to calculate the multiple users' total rates for the uplink and downlink, when the powers of the desired signals, self-interference signals, and noise are known.

### B. Configuration

In the calculation, we assume that the signals come from or reach the broadside direction of the antenna array over a sphere, i.e.,  $\theta \in [0^\circ, 70^\circ]$  and  $\phi \in [0^\circ, 360^\circ]$ . Here, we only consider  $\mathbf{H}_{\text{self}}$  as coming from the mutual coupling between antennas. The non-line-of-sight components due to ambient bounces are neglected in our calculations. We can therefore estimate  $\mathbf{H}_{\text{self}}$  by the measured S-parameters of the antenna array. Only one uplink user and one downlink user are considered for calculation simplification, i.e.,  $K_{\text{up}} = K_{\text{down}} = 1$ . The thermal noise floor is  $-90$  dBm, where the signal bandwidth is assumed to be 100 MHz. The noise dynamic range ratio  $K$  is  $-25$  dBc. The total output power of the antenna array in the base station is 0 dBm, and the output power of the user equipment is  $-10$  dBm. Additionally, we have  $N_{\text{up}} = M_{\text{up}}$ , meaning no self-interference cancellation on the receiving side of the base station.

### C. Achievable Rate Calculation

We calculate the achievable Rates for in-band full duplex with self-interference reduction using eigen-beamforming (SVD-IBFD), as described in Section III-A. For comparison,

we also compute the channel capacities for in-band full duplex with perfect self-interference reduction (Bound-IBFD), in-band full duplex without self-interference reduction (No-IBFD), and half duplex (HALF) as reference points.

1) *Change  $N_{\text{down}}$* : We place  $5 \times 10$  antenna elements in the  $300 \times 600$  mm<sup>2</sup> area, comprising 50 antenna feeds for downlink and 50 antenna feeds for uplink in the in-band full-duplex configuration, and 100 antenna feeds for both uplink and downlink in the half-duplex configuration. We then change  $N_{\text{down}}$  from 1 to 50. The users for both uplink and downlink are located 200 m away from the base station array. It can be seen from Fig. 7 that the Bound-IBFD represents the upper boundary of the in-band full duplex, while the No-IBFD represents the lower boundary. The half-duplex configuration provides a medium level for uplink, downlink, and sum rates. The SVD-IBFD exhibits increasing and decreasing trends for uplink and downlink, respectively. When  $N_{\text{down}} = 22$ , SVD-IBFD yields the largest value, close to the Bound-IBFD.

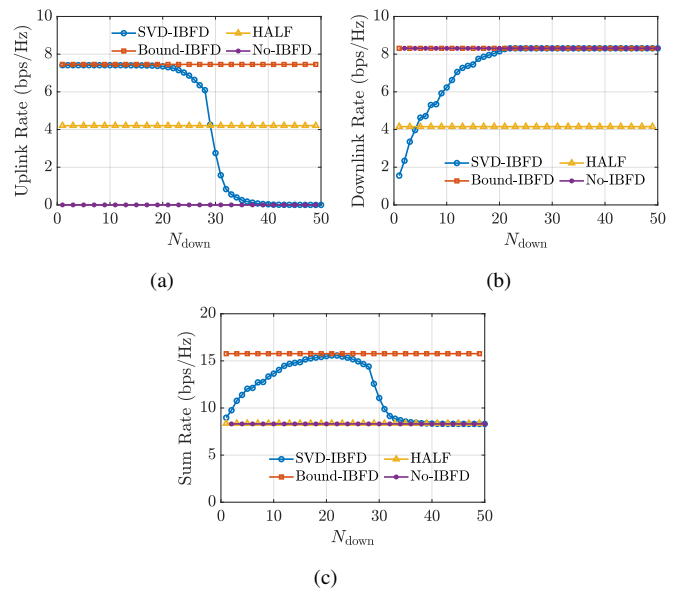


Fig. 7. (a) Uplink rates, (b) downlink rates, and (c) sum rates with different  $N_{\text{down}}$ .

2) *Change  $M_{\text{up}}$  and  $M_{\text{down}}$* : We change the number of antenna elements from  $1 \times 2$  to  $6 \times 12$ , i.e.,  $M_{\text{up}} = M_{\text{down}} = 2, 8, 18, 32, 50, 72, 98$ , and calculate their rates with SVD-IBFD, Bound-IBFD, No-IBFD, and HALF modes. When calculating SVD-IBFD rates, we obtain the maximum rate and its relevant  $N_{\text{down}}$ . In Fig. 8, we can find that the sum rate is highest when spacing  $d_0 \approx 0.5\lambda_0$ . When the number of antennas is large enough, the SVD-IBFD can provide the sum rate as the Bound-IBFD, as shown in Fig 8(c).

### D. Scalability

We also change the user distance to 500 m and the base station output power to  $-10$  dBm. We still find that the spacing  $d_0 \approx 0.5\lambda_0$  can provide the largest sum rates for SVD-IBFD, Bound-IBFD, No-IBFD, and HALF modes. To determine whether the obtained trends of rates are general for each frequency, we also change the antenna elements within a fixed area of  $100 \times 200$  mm<sup>2</sup> at 7.5 GHz. A similar trend

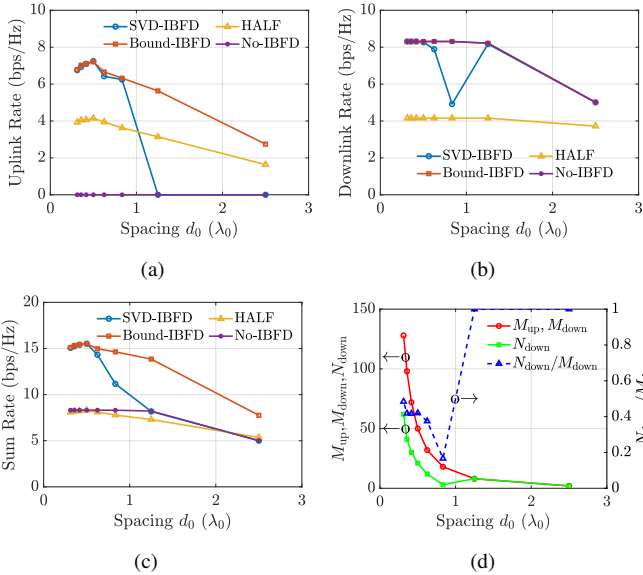


Fig. 8. (a) Uplink rates, (b) downlink rates, and (c) sum rates, and (d)  $M_{up}$ ,  $M_{down}$ , and  $N_{down}$  with different spacing  $d_0$ .

can be observed at 7.5 GHz. Due to page limitations, we do not show them here.

#### IV. MEASUREMENTS OF ANTENNA ARRAY

##### A. Fabrication

Because of the limitations of our measurement equipment,  $300 \times 600 \text{ mm}^2$  is too large for antenna radiation measurements in the Starlab at Aalto University, which measures antenna patterns based on near-field spherical scanning with multiple probes. Additionally, 7.5 GHz is out of the frequency range of the system. Therefore, we finally scale the antenna element to operate at 3.6 GHz. The relevant parameters for each antenna element are listed as follows:  $g_0 = 1 \text{ mm}$ ;  $W_0 = 3 \text{ mm}$ ;  $L_0 = 3.65 \text{ mm}$ ;  $C_0 = 2 \text{ mm}$ ;  $W_1 = 0.5 \text{ mm}$ ;  $g_1 = 6.1 \text{ mm}$ ;  $g_2 = 8.3 \text{ mm}$ ;  $L_1 = 8.4 \text{ mm}$ ;  $L_2 = 13.5 \text{ mm}$ ;  $C_1 = 0.94 \text{ mm}$ ;  $W_2 = 0.5 \text{ mm}$ ;  $H_0 = 20.8 \text{ mm}$ . We fabricated an antenna array with 100 feeds within a  $220 \times 430 \text{ mm}^2$  area. Therefore, the spacing  $d_0$  between elements is around  $0.5\lambda_0$  at 3.6GHz, as shown in Fig. 9.

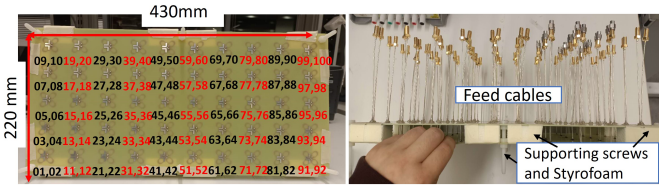


Fig. 9. Fabricated prototype of  $5 \times 10$  antenna array within  $220 \times 430 \text{ mm}^2$ .

##### B. Measurements

1) *S-parameter Measurements*: A 2-port vector network analyzer (VNA) is used to measure the S-parameters. When two ports are connected to the VNA, the other ports are terminated by  $50 \Omega$  loads. Measuring the full S-parameter matrix of 100 ports is time-consuming; therefore, we only

measured some ports' reflection coefficients and mutual coupling levels. The reflection coefficients of the  $50 \Omega$  loads are  $< 29 \text{ dB}$  in the frequency range of interest. The thermal noise level is  $< -120 \text{ dB}$  when the intermediate frequency is 100 Hz. When measuring the mutual coupling levels, some absorbers are used to reduce environmental reflections. Fig. 10(a) shows the measured reflection coefficients for some representative ports, and the simulated reflection coefficients for Port 66 are also displayed, representing the majority of the ports' reflection coefficients. A resonance frequency shift due to fabrication tolerances can be seen in the measured curves. Fig. 10(b) illustrates the mutual coupling levels for different distances between two ports. The mutual coupling level between the farthest two ports, i.e., Port 1 and Port 100, is around  $-60 \text{ dB}$  at 3.6 GHz. It can be observed that the measured curves exhibit similar levels to the simulated ones, demonstrating good agreement. The low-level measured curves show some ripples due to environmental reflections and imperfect absorbing materials.

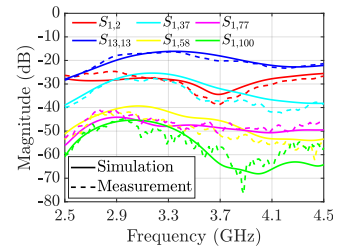


Fig. 10. Fabricated antenna array's (a) reflection coefficients and (b) mutual coupling levels.

2) *Radiation Pattern Measurements*: All 100 antennas' radiation patterns were measured in the StarLab at Aalto University using the setup shown in Fig. 11(a), where the antenna under test (AUT) is connected to the feeding cable, while the other antennas are terminated by  $50\Omega$  loads. The measured and simulated total efficiencies are displayed in Fig. 11(b). It can be observed that the measured efficiencies are approximately 5% lower than the simulated ones because the losses from the feeding thin cables are not included in the simulation model. Some representative radiation patterns are

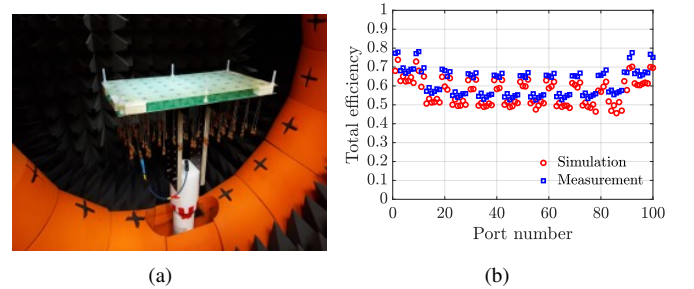


Fig. 11. (a) Setup for radiation pattern measurement; (b) total efficiencies of all antennas in the fabricated antenna array.

shown in Fig. 12. A good agreement is observed between the simulation and measurement, especially for the main beams of the radiation patterns.

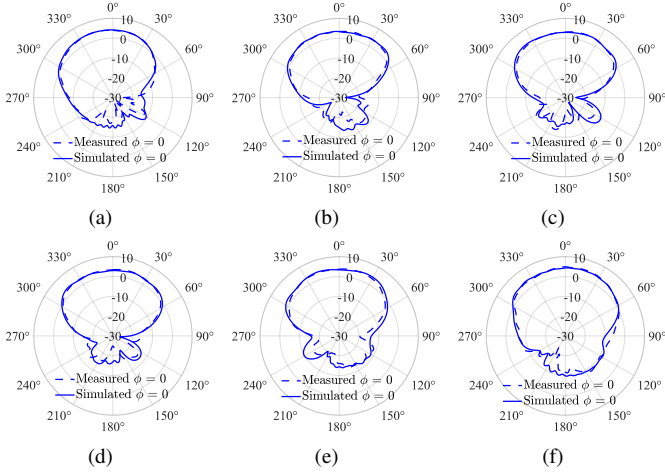


Fig. 12. 2D cut of radiation pattern for (a) Port 7, (b) Port 23, (c) Port 37, (d) Port 57, (e) Port 78, and (f) Port 100 at 3.6 GHz.

### C. Achievable Rate Calculation

The same setups as at 2.6 GHz are used for 3.6 GHz. The uplink and downlink user distances are 200 m from the base stations. The channel capacities with different numbers of effective downlink antennas are calculated, as shown in Fig. 13. The measured curves are derived using the measured

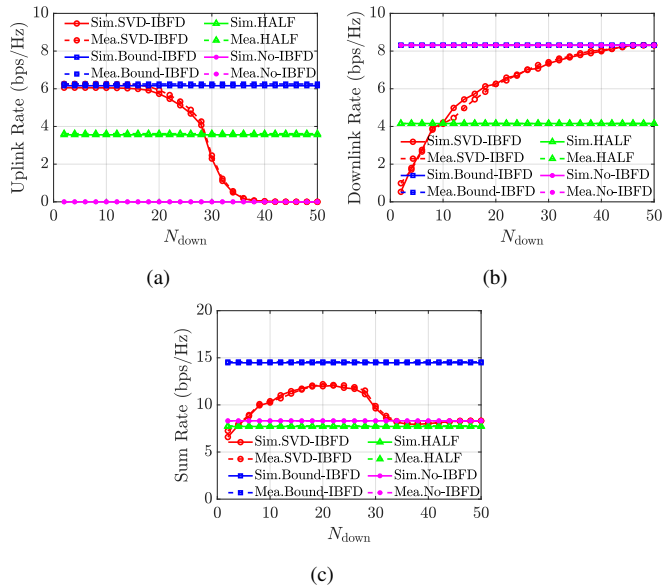


Fig. 13. (a) Uplink rates, (b) downlink rates, and (c) sum rates with different  $N_{\text{down}}$  at 3.6 GHz.

radiation patterns with compensated total efficiencies, which are obtained by the difference between the simulated and measured curves in Fig. 11(b). Fig. 10 shows that the measured S-parameters of selected ports are very similar to the simulated ones. In order to reduce the measurement workload, we assume that all the ports' measured S-parameters are similar to the simulated ones. We use the simulated S-parameters to derive the measured curves. The obtained rate curves are shown in Fig. 13. It can be seen that the measured curves

agree with the simulated ones for SVD-IBFD, Bound-IBFD, No-IBFD, and HALF modes.

## V. CONCLUSIONS

This paper calculates the achievable rates of an in-band full duplex antenna array within a limited area by varying numbers of antenna elements. Through full-wave simulations, the dipole array with  $\pm 45^\circ$  distributions provides the lowest mutual coupling levels. The full-wave simulation results at 2.6 GHz indicate that a  $0.5\lambda_0$  element spacing yields the largest achievable rates for the in-band full duplex mode. When extending the calculations to different user distances and 7.5 GHz, similar results are observed. For the achievable rates calculation using the fabricated antenna array operating at 3.6 GHz, the results obtained with measured radiation patterns show excellent agreement with those calculated using simulated ones, further justifying the study's conclusions.

## VI. ACKNOWLEDGEMENT

Part of the results are obtained through NokiaXG doctoral school funding supported by Nokia Mobile Network.

## REFERENCES

- [1] A. Nagulu, N. Reiskarimian, T. Chen, S. Garikapati, I. Kadota, T. Dinc, S. L. Garimella, M. Kohli, A. S. Levin, G. Zussman, and H. Krishnaswamy, "Doubling down on wireless capacity: A review of integrated circuits, systems, and networks for full duplex," *Proceedings of the IEEE*, vol. 112, no. 5, pp. 405–432, 2024.
- [2] E. Everett, C. Shepard, L. Zhong, and A. Sabharwal, "Softnull: Many-antenna full-duplex wireless via digital beamforming," *IEEE Transactions on Wireless Communications*, vol. 15, no. 12, pp. 8077–8092, 2016.
- [3] E. Aryafar, M. A. Khojastepour, K. Sundaresan, S. Rangarajan, and M. Chiang, "MIDU: Enabling MIMO full duplex," in *Proceedings of the 18th annual international conference on Mobile computing and networking*, 2012, pp. 257–268.
- [4] M. Duarte and G. C. Alexandropoulos, "Full duplex mimo digital beamforming with reduced complexity auxtx analog cancellation," in *ICC 2020 - 2020 IEEE International Conference on Communications (ICC)*, 2020, pp. 1–6.
- [5] S. Huberman and T. Le-Ngoc, "Mimo full-duplex precoding: A joint beamforming and self-interference cancellation structure," *IEEE Transactions on Wireless Communications*, vol. 14, no. 4, pp. 2205–2217, 2014.
- [6] E. Balti, S. Akoum, I. Alfalujah, and B. L. Evans, "Hybrid beamforming design for full-duplex millimeter wave massive mimo systems," *IEEE Transactions on Vehicular Technology*, 2024.
- [7] L. Li, M. Ali, and K. Haneda, "Compact dual-band antenna array for massive mimo," in *2016 IEEE 27th Annual International Symposium on Personal, Indoor, and Mobile Radio Communications (PIMRC)*, 2016, pp. 1–6.
- [8] W. Huang, Y. He, W. Li, L. Zhang, S.-W. Wong, and Z. Zeng, "A low-profile dual-polarized wideband antenna for 5g massive mimo base station," in *2021 IEEE International Workshop on Electromagnetics: Applications and Student Innovation Competition (iWEM)*. IEEE, 2021, pp. 1–3.
- [9] Y. He, J. Li, C. Li, L. Zhang, and S.-W. Wong, "A novel base station antenna element for 3g/4g/sub-6 ghz 5g applications," in *2019 8th Asia-Pacific Conference on Antennas and Propagation (APCAP)*. IEEE, 2019, pp. 581–583.
- [10] B. Wang, C. Liao, and C.-H. Du, "A low-profile broadband dual-polarized base station antenna array with well-suppressed cross-polarization," *IEEE Transactions on Antennas and Propagation*, vol. 69, no. 12, pp. 8354–8365, 2021.
- [11] B. T. Quist and M. A. Jensen, "Optimal antenna radiation characteristics for diversity and mimo systems," *IEEE Transactions on Antennas and Propagation*, vol. 57, no. 11, pp. 3474–3481, 2009.
- [12] T. Riihonen, A. Balakrishnan, K. Haneda, S. Wyne, S. Werner, and R. Wichman, "Optimal eigenbeamforming for suppressing self-interference in full-duplex mimo relays," in *2011 45th Annual Conference on Information Sciences and Systems*. IEEE, 2011, pp. 1–6.